Optimal Estimation and Detection in Homogeneous Spaces

Raman Arora, *Member, IEEE*, and Harish Parthasarathy

***Abstract*—This paper presents estimation and detection techniques in homogeneous spaces that are optimal under the squared error loss function. The data is collected on a manifold which forms a homogeneous space under the transitive action of a compact Lie group. Signal estimation problems are addressed by formulating Wiener-Hopf equations for homogeneous spaces. The coefficient functions of these equations are the signal correlations which are assumed to be known. The resulting coupled integral equations on the manifold are converted to Wiener-Hopf convolutional integral equations on the group. These are solved using the Peter-Weyl theory of Fourier transform on compact Lie groups. The computational complexity of this algorithm is reduced using the bi-invariance of the correlations with respect to a stabilizer subgroup. The theory of matched filtering for isotropic signal fields is developed for signal classification where given a set of template signals on the manifold and a noisy test signal, the objective is to optimally detect the template buried in the test signal. This is accomplished by designing a filter on the manifold that maximizes the signal-to-noise-ratio (SNR) of the filtered output. An expression for the SNR is obtained as a ratio of quadratic forms expressed as Haar integrals over the transformation group. These integrals are expressed in the Fourier domain as infinite sums over the irreducible representations. Simplification of these sums is achieved by invariance properties of the signal function and the noise correlation function. The Wiener filter and matched filter are developed for an abstract homogeneous space and then specialized to the case of spherical signals under the action of the rotation group. Applications of these algorithms to denoising of 3D surface data, visual navigation with omnidirectional camera and detection of compact embedded objects in the stochastic background are discussed with experimental results.**

***Index Terms*—Homogeneous spaces, Wiener filter, matched filter, spherical harmonics, surface smoothing, visual homing, cosmological microwave background data.**

I. Introduction

With the advances in modern acquisition devices, large volume of experimental data on high-dimensional nontrivial manifolds is readily available. In astrophysics and cosmology, the cosmic microwave background (CMB) radiation is collected in all directions of the sky on the celestial sphere [1]. In geophysics, remote sensing of the Earth's surface and atmosphere generates spherical data maps which are crucial for understanding climatic changes, geodynamics or monitoring human-environment interactions. In robotics, omnidirectional cameras capture the three-dimensional (3D) scene on a parabolic or hyperbolic mirror which can be mapped onto a regular spherical grid [2], [3]. The 3D scene may also be captured on the sphere using a pair of fisheye lenses [4]. A real-time omnidirectional camera incorporating a catadioptric module as well as a fisheye module, thereby providing a full spherical field of view, was presented in [5]. These vision systems find applications in robotics [6], video surveillance, medical imaging and automatic face recognition. Various localization and motion-estimation or motion-recovery techniques in robotics employ omnidirectional imagery [6]–[9]. In many settings, however, the data is available on arbitrary manifolds. In biomedical imaging and computer vision, 3D surface data is acquired with range scanners or stereovision systems. If the data corresponds to *star-shaped* objects (objects with surfaces topologically isomorphic to the sphere), it may be considered to be a height field on the sphere [10]. Another approach is to use triangular meshes to model such complex shapes and employ local parametrization to transform the surface mesh into a spherical signal [11]. Some researchers have also explored conformal maps [12] and isometric embedding of 3D surfaces on the sphere [13].

The analysis and processing of such complex data requires new and sophisticated signal processing techniques in various different settings. Often, the development of such methods benefits from learning inherent structure present in the data due to the physics of the underlying generative mechanism. Group theory is the natural choice for capturing the structure in data by describing the transformations that act on the data. This is also evident from recent emphasis on algorithms that better exploit differential geometry and computational topology [14]–[16]. For a nice introduction to the role of group theory and differential geometry in signal processing, see [17] and [18].

Inspired by a multitude of applications of signal processing in nontrivial signal spaces, the basic algorithms are generalized to abstract homogeneous spaces. For signal estimation, a Wiener filter is derived. This finds application in denoising of images as well as in reconstruction from a sparse set of samples. A spherical Wiener filter is applied for denoising 3D surfaces. A few researchers have previously employed spherical diffusion techniques [10] or filtering [11] for smoothing and denoising 3D surface data but the filters used were smooth Gaussian kernels with low-pass characteristics. The Wiener filter is optimal in the minimum mean-squared-error (MMSE) sense and, thus, results in better reconstruction and denoising for omnidirectional images and 3D surface data that can be represented as functions or

Manuscript received February 01, 2009; accepted November 16, 2009. First published January 15, 2010; current version published April 14, 2010. The associate editor coordinating the review of this manuscript and approving it for publication was Prof. Jean-Christophe Pesquet.

R. Arora was with the University of Wisconsin, Madison, WI 53706 USA. He is now with the University of Washington, Seattle, WA 98195 USA (e-mail: rmnarora@u.washington.edu).

H. Parthasarathy is with the Department of Electronics and Communication Engineering, Netaji Subhas Institute of Technology, Delhi, India.

Color versions of one or more of the figures in this paper are available online at http://ieeexplore.ieee.org.

Digital Object Identifier 10.1109/TSP.2010.2040687

images on the sphere. However, it relies on prior knowledge of second-order signal statistics. In the absence of such information one may estimate it from the given observations or assume a model for the associated power spectral density. Our work on Wiener filtering is closely related to prior work on deconvolution over groups [19].

For signal classification, a matched filter is derived for isotropic signal fields. A matched filter for spherical signals is applied for visual navigation of an autonomous robot and for detecting compact objects embedded in a stochastic background. The spherical matched filter is also motivated by recent biological findings that the human visual system incorporates rotation and pose invariance in recognition. Furthermore, the localization and navigation tasks have been suggested to be based on matched filters implemented by neurons that have spherical receptive fields [20].

The paper is organized as follows. The Wiener filtering and matched filtering problems are formulated for homogeneous spaces in Section II. The theory is developed in complete generality for functions defined on a manifold M under the transitive action of a compact Lie group G. Section III provides mathematical preliminaries in group theory and representation theory. The stochastic component of the signal field is assumed to be isotropic which implies that the correlation functions are G-stationary. The computational complexity of the algorithms can thus be reduced by exploiting the invariance of the image correlations with respect to a stabilizer subgroup of the transformation group as discussed in Section IV. Section V presents a solution to the Wiener-Hopf equations in a homogeneous space. These equations comprise a set of coupled linear integral equations that are expressed as convolutional integral equations on the transformation group. The integral equations are expressed in the Fourier domain as discrete sums over the irreducible representations of the compact Lie group using the Peter-Weyl theory [21]. The Wiener filter is simplified using the complexity reduction technique of Section IV.

Section VI presents an expression for the impulse response of the matched filter described in terms of the Fourier coefficients of the template normalized by the variance of the noise projected onto the corresponding representation spaces. The expression for the signal-to-noise-ratio (SNR) is obtained as a ratio of quadratic forms in the filter impulse response. Each of these quadratic forms is expressed as a Haar integral over the transformation group. These integrals are then expressed in the Fourier domain as infinite sums over the irreducible representations of the compact Lie group. The sums involve: (a) the signal Fourier components; (b) the filter Fourier components; and (c) the noise spectral density matrix entries. Simplification of these sums is achieved by using invariance properties of the signal function and the noise correlation function with respect to a stabilizer subgroup. For spherical matched filter this amounts to matrix sums being converted into vector sums. The matched filter is obtained by application of the Cauchy-Schwarz inequality to this ratio. The optimum filter is finally expressed in polar coordinates using spherical harmonics. Various applications of the algorithms specialized to spherical signals are discussed in Section VII with experimental results. Some parts of the paper have appeared in [22] and [23].

II. Problem Formulation

In many signal processing applications, data typically comes in the form of a point cloud sampled from a surface embedded in a high dimensional Euclidean space. The topological and geometric properties inherited from the underlying manifold structure are better exploited by developing data-processing methods with the manifold assumption rather than application of existing approaches to the point cloud data in the Euclidean space. Furthermore, the transformations of the data can often be described by a compact Lie group acting transitively on the manifold, resulting in a *homogeneous space*. The focus in this paper is on such signal spaces. The classic example of a homogeneous space is the Euclidean space under the action of the translation group. A non-trivial example is the rotation group acting on the unit sphere.

Let M denote a manifold and let G be a compact Lie group[1] of transformations acting transitively on M. Consider a real-valued random field $\{\xi(x) : x \in M\}$ defined on the manifold M. This is typical of most signal processing and computer vision problems where the manifold corresponds to a curve or surface and the group corresponds to various transformations like rotations, projections, etc. The signal field comprises a non-random signal component s and a noise component r

$$\xi(x) = s(x) + r(x), \quad x \in M.$$

The noise is assumed to be isotropic, i.e., the correlation function $K(x_1, x_2) = \mathbb{E}[r(x_1)r(x_2)]$, satisfies the group invariance

$$K(g \cdot x_1, g \cdot x_2) = K(x_1, x_2)$$

for all $x_1, x_2 \in M$ and $g \in G$. This implies that the autocorrelation function of the random process r does not vary under the transformations of the manifold. The isotropic assumption in a homogeneous space is equivalent to the notion of wide sense stationarity in Euclidean spaces. This is a standard observation model in most signal processing paradigms.

A *filter on the manifold* M is an operator, h, that sends the signal ξ on M to $\eta = \int_M h(x)\xi(x)dx$ on M where $dx = \nu(dx)$ is the invariant measure on M induced by G. Note that integration with respect to any measure that is absolutely continuous with respect to dx can be reduced to integration with respect to dx by appropriately modifying the filter. Assuming that h is square integrable with respect to dx (i.e., $\int_M |h(x)|^2 dx < \infty$), the filter can be regarded as a continuous map $h : \mathscr{L}^2(M) \to \mathscr{L}^2(M)$ that maps the space of square integrable signals on M to itself. Boundedness (bounded input, bounded output) follows from

$$\mathbb{E}\left|\int_M h(x)\xi(x)dx\right|^2 \leq \int_M |h(x)|^2 dx \cdot \int \mathbb{E}[|\xi(x)|^2]dx.$$

A. Wiener Filtering

In practical applications, the data collected is either noisy or incomplete and an important preprocessing step is to infer the

[1]See Section III for definitions.

missing information or clean up the data based on the given samples. The Wiener filter generates the optimal linear estimates for the missing information or denoised data based on the observations and prior knowledge of the signal correlations. Consider a collection of $k+1$ real-valued random processes $\{\eta_1(x),\ldots,\eta_k(x),\xi(x)|x\in M\}$. The variables η_i's denote the k observations or examples on the manifold and ξ denotes the unobserved signal that needs to be reconstructed based on these observations. For instance, in biomedical imaging, η_i's may represent images of a 3D object at depths d_i's and may be used as reference processes to estimate the image ξ at an unobserved depth d. For more details on application to imaging systems, refer to [22].

The random processes are assumed to be zero mean, i.e., $\mathbb{E}[\xi(x)]=0, \mathbb{E}[\eta_i(x)]=0$, and jointly wide sense G-stationary, i.e., the correlation functions satisfy

$$\begin{aligned}\mathbb{E}[\xi(x)\bar{\xi}(y)] &= R(x,y)=R(g\cdot x, g\cdot y)\\ \mathbb{E}[\xi(x)\bar{\eta}_j(y)] &= R_j(x,y)=R_j(g\cdot x, g\cdot y)\\ \mathbb{E}[\eta_i(x)\bar{\eta}_j(y)] &= R_{ij}(x,y)=R_{ij}(g\cdot x, g\cdot y)\end{aligned} \tag{1}$$

for all $g\in G, x,y\in M$ and $i,j=1,\ldots,k$. Note that $\bar{\xi}$ denotes the complex conjugate of ξ. The best linear estimate $\hat{\xi}(x)$ of the process $\xi(x)$ based on η_i's is

$$\hat{\xi}(x)=\sum_{i=1}^{k}\int_M L_i(x,y)\eta_i(y)dy \tag{2}$$

where integration is with respect to the unique G-invariant measure on the compact manifold M and L_i are unknown functions to be determined that minimize the MSE $\mathbb{E}|\xi(x)-\hat{\xi}(x)|^2$. To ensure that $\hat{\xi}(x)$ is a G-stationary process, $L_i(x,y)$ should be G-invariant, i.e., $L_i(g\cdot x, g\cdot y)=L_i(x,y)$ for $g\in G$, $x,y\in M$.

Wiener filtering is applied in Section VII to 3D surface denoising and used as a preprocessing step in the detection of compact embedded objects in noisy sky maps obtained from the CMB data.

B. Matched Filtering

In signal processing tasks like face recognition or radar, we are given class examples or templates and the goal is to perform m-ary classification on a test sample. A matched filter correlates the test signal with a given template to test for the presence of the template in the unknown signal. It is an optimal detector in additive noise since it maximizes the output SNR. Consider a finite set of templates $\Xi=\{\xi_1(x),\ldots,\xi_m(x)|x\in M\}$, and a test signal ξ comprising an unknown template buried in noise

$$\xi(x)=s(x)+r(x),\quad x\in M$$

where $s\in\Xi$. To identify the unknown template buried in isotropic noise r, the test signal is cleaned by passing through a filter h. The filtered output sampled at a fixed point $y\in M$ is given as

$$\eta(y)=\int_M h(x,y)\xi(x)\,(dx).$$

Suppressing the variable y for notational convenience, the signal and noise components of the filtered output are denoted as

$$\eta_s=\int_M h(x)s(x)dx, \eta_r=\int_M h(x)r(x)dx. \tag{3}$$

The objective is to design the filter h that maximizes the SNR

$$\mathrm{SNR}(h)=\frac{|\eta_s|^2}{\mathbb{E}|\eta_r|^2}. \tag{4}$$

With multiple templates, a bank of filters matched to the given templates is designed and the template corresponding to the maximum output SNR is picked. Matched filtering is employed in Section VII to detect compact embedded objects in the sky maps given by the CMB data and also for visual homing of robots.

III. Mathematical Preliminaries

Inspired by the group theoretical methods in image processing [21], [24], the problems of Wiener filtering and matched filtering are addressed using the harmonic analysis based on the irreducible representations of the group G. This section introduces the reader to the group representations and the Peter-Weyl theorem that is at the heart of the analysis in this paper.

A. Group Representations

Groups are mathematical entities that allow us to study symmetries. They were originally defined to be transformations of sets, like symmetries of a geometric object or linear transformations of vector spaces [25]. Over the last century they have come to evolve as abstract objects which can be represented as a group of transformations. This is precisely what group representations facilitate. For the sake of simplicity, in this paper we will restrict ourselves to linear representations of compact Lie groups.

Formally, a group is a set of elements with a binary operation that is closed and associative and admits a unique identity element and an inverse for every element of the set. A *topological group* is a group with a topology that is compatible with the group structure, i.e., the binary operation and the inversion map are continuous functions. For instance, the n-dimensional Euclidean space $\mathbb{R}^n$ endowed with the standard topology forms a topological group under vector addition. A *Lie group* is a topological group that is also a finite-dimensional smooth manifold. An important example of a Lie group is the general linear group $\mathrm{GL}(n)$ of invertible matrices of size $n\times n$. A compact group is a topological group that is also a compact space. An example of a compact group is the rotation group $\mathbf{SO}(n)$ of $n\times n$ orthogonal matrices with determinant $+1$.

A *group homomorphism* is a map π from a group $(G,\cdot)$ into another group $(H,\circ)$ such that $\pi(g_1\cdot g_2)=\pi(g_1)\circ\pi(g_2)$ for all $g_1,g_2\in G$. For instance, consider the group of rotations in 3D Euclidean space about the origin. These rotations can be represented by the group of 3×3 orthogonal matrices with unit determinant. And the composition of two rotations is described simply by matrix multiplication. Thus the matrix group $\mathbf{SO}(3)$ provides a representation for the 3D rotation group.

Group representations are descriptions of elements of abstract groups as invertible matrices. This allows the group-operation to be described as matrix multiplication and the abstract group as linear transformations of vector spaces. Many group-theoretic problems can therefore be studied as simple problems in linear algebra. To get a picture, consider the vector space V of homogeneous polynomial of degree j on the sphere (in two variables). The rotation of the sphere takes a given polynomial

$p \in V$ to the rotated version $p' \in V$. Since V is finite dimensional, the rotation can be described by a linear transformation matrix of size $j \times j$. A representation in this case is defined to be the map that assigns a linear invertible matrix to every element of the rotation group. Furthermore, the collection of homogeneous polynomials for all degrees $j \geq 0$ provides a basis for the function space of analytical functions on the unit sphere. Thus the study of representations helps describe the group action on the space of functions on the homogeneous space.

Formally, a representation π of a group G on a vector space V_π is a homomorphism from G to the group of all bijective linear transformations of the vector space V_π. The dimension d_π of the representation π is defined to be the dimension of the representation space V_π. Given a finite dimensional representation, for every $g \in G, \pi(g)$ can be thought of as a $d_\pi \times d_\pi$ invertible matrix operating on V_π. The entries of the matrix are given by continuous functions $\pi_{\alpha,\beta}(g)$, for $\alpha, \beta \in \{1, 2, \ldots, d_\pi\}$. An example of a one-dimensional representation of the planar rotation group $\mathbf{SO}(2)$ is the exponential map that takes rotations in the plane to the multiplicative group of complex numbers $(\mathbb{C}, \times)$. Two elements g_1, g_2 of $\mathbf{SO}(2)$ that correspond to rotations θ_1, θ_2 are given by phasors $e^{j\theta_1}, e^{j\theta_2}$ respectively. The homomorphism follows from the identity $e^{j\theta_1} \cdot e^{j\theta_2} = e^{j(\theta_1+\theta_2)}$.

Two representations are said to be *equivalent* if for all elements of the group, the matrices under two representations are similar. Formally, if π_1, π_2 are two representations of a group G, then π_1 and π_2 are equivalent if there exists an invertible matrix S such that for all $g \in G, \pi_1(g)\ S = S\ \pi_2(g)$. Since it is possible to map two equivalent representation spaces by a simple *change-of-basis* we can regard two equivalent representations to be the same. A representation is said to be *irreducible* if the representation matrix cannot be block-diagonalized simultaneously for all group elements. A *reducible* representation can be described as a direct sum of other representations whereas an irreducible representation has no proper invariant subspaces. Finally, a representation π is said to be unitary if $\pi(g)$ is a unitary matrix for all $g \in G$.

The classification of the complete set of irreducible inequivalent unitary representations (IURs) of a group is fundamental to the harmonic analysis on the group. For commutative groups, all IURs are one-dimensional whereas non-commutative groups can admit higher dimensional representations. Harmonic analysis on the group entails describing the decomposition of any arbitrary unitary representation of the group into inequivalent irreducible unitary representations. This decomposition extends naturally to the space of functions defined on the group. However, analysis requires a notion of invariant measure on the subsets of the group. Fortunately, such a measure exists for all compact topological groups and is called the Haar measure. Subsequently, the integrals of functions on groups are well defined. Peter-Weyl theorem describes the decomposition of the space of square integrable functions on compact groups into invariant subspaces associated with IURs.

B. Peter-Weyl Theory

Let G be a compact group and let dg denote the Haar measure associated with G. Let $\hat{G}$ denote the dual space of G, i.e., the set of all inequivalent irreducible unitary representations of G. For compact groups, the dual space $\hat{G}$ is countable and every irreducible representation is finite-dimensional. The Peter-Weyl theorem states that $\{\sqrt{d_\pi}\pi_{\alpha,\beta}(g) | 1 \leq \alpha, \beta \leq d_\pi, \pi \in \hat{G}\}$ is a complete orthonormal basis for $\mathscr{L}^2(G)$, the space of all square integrable functions on G. Thus, any $f \in \mathscr{L}^2(G)$ can be expanded in this basis as,

$$f(g) = \sum_{\pi \in \hat{G}} \sum_{1 \leq \alpha, \beta \leq d_\pi} d_\pi \langle f, \pi_{\alpha\beta} \rangle \pi_{\alpha\beta}(g) \tag{5}$$

where

$$\langle f, \pi_{\alpha\beta} \rangle = \int_G f(g) \bar{\pi}_{\alpha\beta}(g) dg.$$

In compact notation, the $d_\pi \times d_\pi$ matrix

$$\hat{f}(\pi) = \int_G f(g) \pi^*(g) dg$$

is defined to be the *Fourier transform* of f at representation (frequency) $\pi \in \hat{G}$. Note that π^* denotes the complex conjugate transpose of the matrix π. Similarly, (5) can be expressed in compact notation as

$$f(g) = \sum_{\pi \in \hat{G}} d_\pi \mathrm{Tr}(\hat{f}(\pi)\pi(g)) \tag{6}$$

where $\mathrm{Tr}(\mathbf{A})$ represents the trace of the matrix $\mathbf{A}$. Equation (6) defines the *inverse Fourier transform* of $\hat{f}$. For two square integrable functions $u, v \in \mathscr{L}^2(G)$ Parseval's relation states,

$$\int_G u(g)\bar{v}(g)\, dg = \sum_{\pi \in \hat{G}} d_\pi\ \mathrm{Tr}(u_\pi v_\pi^*). \tag{7}$$

C. Expressing Integrals on Manifold as Integrals on the Group

Often it is convenient in a homogeneous space to make a variable substitution so that a function defined on the manifold can be expressed as a function on the group acting transitively on the manifold. This will allow the signals defined on the manifold to be expanded in Fourier series as in (6). Also, the integrals (or convolutions) on the manifold can be expressed as integrals on the group. The following elementary but useful measure theoretic result allows for such substitutions.

Let x_0 be a fixed point on the manifold M and consider a measurable map τ from the measure space $(G, \mathscr{F}_G, \mu)$ to the measure space $(M, \mathscr{F}_M, \nu)$ given by $\tau(g) = g \cdot x_0$. Note that $\mathscr{F}_G$ is the Borel sigma-algebra associated with the standard topology on the group G and $\mathscr{F}_M = \{E \subseteq M | \tau^{-1}(E) \in \mathscr{F}_G\}$ is the sigma-algebra induced on M. Also, μ is the natural Haar measure associated with the compact group G and ν is the G-invariant measure on M induced by τ (for $E \in \mathscr{F}_M$ define $\nu(E) = \mu(\tau^{-1}(E))$). Therefore, if f is a measurable function on M that is integrable with respect to ν then $f \circ \tau$ is integrable with respect to μ and

$$\int_M f(x)\nu(dx) = \int_G f(g \cdot x_0)\mu(dg).$$

Finally, since the action of G on M is transitive, there exists a measurable cross-section map $\gamma : M \to G$ such that $\gamma(x)\cdot x_0 = x$ for all $x \in M$. This allows for the reverse substitution: if f is a square integrable function on M then it can be developed into a Fourier series over G,

$$f(x) = \sum_{\pi \in \hat{G}} d_\pi \mathrm{Tr}(\hat{f}(\pi)\pi(\gamma(x))), \quad x \in M. \tag{8}$$

IV. Complexity Reduction

This section presents the first main result of the paper that allows the reduction of complexity of algorithms developed in later sections. Fix a point x_0 on the manifold M; call it the 'origin'. Consider the *stabilizer* of x_0, i.e., the set of all transformations in the group G that leave the origin fixed,

$$H = \{h \in G : h \cdot x_0 = x_0\}.$$

H is a closed subgroup of G and has its own Haar measure μ_H. A function f on G is said to be *H-invariant* if $f(gh) = f(g)$ for all $g \in G$ and $h \in H$. A function f on G is said to be *H-bi-invariant* if $f(h_1 g h_2) = f(g)$ for all $g \in G$ and $h_1, h_2 \in H$. We have the following result for such functions.

Theorem 1: The Fourier transform of an H-invariant function f satisfies the relation $P_\pi \hat{f}(\pi) = \hat{f}(\pi)$ for every $\pi \in \hat{G}$, where

$$P_\pi = \int_H \pi(h)\mu_H(dh)$$

is the orthogonal projection onto

$$W_\pi = \{x \in V_\pi : \pi(h)x = x \; \forall \, h \in H\}.$$

For an H-bi-invariant function $f, P_\pi \hat{f}(\pi) P_\pi = \hat{f}(\pi)$.

Proof: See Appendix IX.B. ∎

The significance of this result is that for H-invariant and H-bi-invariant functions, the Fourier transform matrix $\hat{f}(\pi)$ lies in a smaller dimension subspace. If d_π^0 denotes the dimension of W_π, then $\hat{f}(\pi)$ has rank d_π^0. Furthermore, restricting $\hat{f}(\pi)$ to an orthonormal basis for W_π, it is seen that $\hat{f}(\pi)$ lives in a subspace of dimension $d_\pi^0 \times d_\pi$ for H-invariant f. For H-bi-invariant f, the Fourier matrix lies in a $d_\pi^0 \times d_\pi^0$ dimensional subspace. This will be exploited in later sections to reduce the size of the problem.

V. Wiener Filtering on Homogeneous Spaces

This section presents the Wiener filter for isotropic signal fields on homogeneous spaces. The MMSE solution comprises a set of coupled linear integral equations on the unit sphere which are solved using the Peter-Weyl theory. The computational complexity of the filter is reduced using the bi-invariance of the signal correlations as discussed in Section IV.

A. Wiener Hopf Equations

As formulated in Section II-A the best linear estimate $\hat{\xi}(x)$ of the process $\xi(x)$ based on η_i's is

$$\hat{\xi}(x) = \sum_{i=1}^{k} \int_M L_i(x,y)\eta_i(y)dy \tag{9}$$

where $L_i(x,y)$ are unknown functions that minimize the mean-squared error (MSE) $\mathbb{E}|\xi(x) - \hat{\xi}(x)|^2$. The orthogonality principle states that the MSE is minimized when $\mathbb{E}[(\xi(x) - \hat{\xi}(x))\bar{\eta}_j(y)] = 0$ for $j = 1, \ldots, k$ and $x, y \in M$. Using (9) and the G-stationary assumptions in (1), the orthogonality principle gives the following normal equations

$$R_j(x,y) = \sum_{i=1}^{k} \int_M L_i(x,z)R_{ij}(z,y)dz \tag{10}$$

for $1 \le j \le k$ and $x, y \in M$. We need to find G-invariant functions that satisfy these coupled linear integral equations on the manifold. These equations can be expressed as relations on the group G as follows. Fix an "origin" x_0 in M. Then, by the transitivity of the group action, there exist $g_1, g_2 \in G$ such that $x = g_1 \cdot x_0$ and $y = g_2 \cdot x_0$. Then (10) can be expressed as

$$R_j(g_1 \cdot x_0, g_2 \cdot x_0) = \sum_{i=1}^{k} \int_M L_i(g_1 \cdot x_0, z)R_{ij}(z, g_2 \cdot x_0)dz. \tag{11}$$

Using the fact that the map $g \mapsto g \cdot x_0$ from G into M takes the normalized Haar measure of G to the unique G-invariant measure on M, the integral in (11) can be transformed into an integral on G (see Section III-C)

$$R_j(g_1 \cdot x_0, g_2 \cdot x_0) = \sum_{i=1}^{k} \int_G L_i(g_1 \cdot x_0, g \cdot x_0)R_{ij}(g \cdot x_0, g_2 \cdot x_0)\, dg \tag{12}$$

for $g_1, g_2 \in G$ where dg indicates integration with respect to the Haar measure on G. It is convenient to use different notation when viewing the correlation functions as functions on the group. Define $\phi_j(g) = R_j(x_0, g\cdot x_0), \psi_{ij}(g) = R_{ij}(x_0, g\cdot x_0)$ and $l_i(g) = L_i(x_0, g\cdot x_0)$. Then using the invariance conditions it is easily verified that for all $g \in G$, (12) can be written as

$$\phi_j(g) = \phi_j\left(g_1^{-1}g_2\right) = \sum_{i=1}^{k} \int_G l_i(g')\psi_{ij}(g'^{-1}g)\, dg'. \tag{13}$$

These equations can be expressed as a matrix convolution

$$\boldsymbol{\phi}^T(g) = \int_G l^T(g')\psi(g'^{-1}g)dg', \quad g \in G \tag{14}$$

in a compact notation where $\phi = [\phi_1, \ldots, \phi_k]^T, l = [l_1, \ldots, l_k]^T$ and $\psi = [\psi_{ij}]_{k\times k}$. Note that these convolutional integral equations are the Wiener-Hopf equations (10), expressed in terms of integrals on the group G. Taking the Fourier transform on both sides of (13) yields the following result.

Lemma 1: The Fourier transform coefficients of the correlation functions ϕ and ψ satisfy the following system of linear equations,

$$\hat{\phi}_j(\pi) = \sum_{i=1}^{k} \hat{\psi}_{ij}(\pi)\, \hat{l}_i(\pi) \tag{15}$$

for $j = 1, \ldots, k$ and $\pi \in \hat{G}$, where $\hat{\phi}_j(\pi) = \int_G \phi_j(g)\pi^*(g)dg$, $\hat{l}_i(\pi) = \int_G l_i(g)\, \pi^*(g)\, dg$ and $\hat{\psi}_{ij}(\pi) = \int_G \psi_{ij}(g)\, \pi^*(g)\, dg$.

Proof: See Appendix IX.C ∎

The system of linear equations in (15) can be solved for the unknown $\hat{l}_i(\pi)$ and the filter response $L_i(x,y)$ is obtained as follows. Given the cross-section $\gamma : M \to G$ discussed in Section III.C, compute

$$\begin{aligned} L_i(x,y) &= L_i(\gamma(x)\cdot x_0, \gamma(y)\cdot x_0) \\ &= L_i(x_0, (\gamma(x)^{-1}\gamma(y))\cdot x_0) \\ &\quad (\text{use } G\text{–invariance}) \\ &= l_i(\gamma(x)^{-1}\gamma(y)) \end{aligned}$$

for $1 \le i \le k$ and $x, y \in M$, where l_i is the inverse Fourier transform of $\hat{l}_i$. The functions $\{L_i(x,y)\}_{i=1}^k$ comprise the Wiener filter and can be used in (9) to obtain the estimates $\hat{\xi}$. However, each of the equations in Lemma 1 involves $d_\pi \times d_\pi$ matrices and solving them is a computational challenge.

B. Complexity Reduction for the Wiener Filter

Solving the system of equations in Lemma 1 for $\hat{l}_i(\pi)$ yields the Wiener filter. However, the computational complexity of the system is large. There are k equations, each of which involves $d_\pi \times d_\pi$ matrices $\hat{\phi}$, $\hat{l}$ and $\hat{\psi}$. Furthermore, $\hat{G}$ is countably infinite and the dimension d_π of the matrices ranges over all positive integers. To efficiently solve for the Wiener filter, the structure and redundancy in Fourier coefficient matrices is exploited. As discussed in Section IV for H bi-invariant functions $f, \hat{f}(\pi)$ lies in a smaller subspace W_π. Denote the restriction of the operator $\hat{f}(\pi)$ to the subspace W_π by $\tilde{f}(\pi)$ and restriction of $P_\pi \pi(g) P_\pi$ to the subspace W_π by $\tilde{\pi}(g)$. Then, $\tilde{f}(\pi)$ and $\tilde{\pi}(g)$ can be thought of as $d_\pi^0 \times d_\pi^0$ matrices in any orthonormal basis of the subspace W_π. Using Theorem 1, any square integrable H-bi-invariant function f on G can therefore be recovered from the operators $\{\tilde{f}(\pi), \pi \in \hat{G}\}$ as

$$f(g) = \sum_{\pi \in \hat{G}} d_\pi \mathrm{Tr}(\tilde{f}(\pi)\tilde{\pi}(g)).$$

Owing to the H-bi-invariance of functions ϕ_j, ψ_{ij} and l_i, the matrices $\tilde{\phi}_j, \tilde{\psi}_{ij}$ and $\tilde{l}_i$ are $d_{\pi_0} \times d_{\pi_0}$ dimensional. Consequently, the system of linear equations in Lemma 1 reduces to

$$\tilde{\phi}_j(\pi) = \sum_{i=1}^k \tilde{\psi}_{ij}(\pi)\tilde{l}_i(\pi), \quad 1 \le j \le k \text{ and } \pi \in \hat{G}. \tag{16}$$

Typically, d_{π_0} is much smaller than d_π.

C. The Spherical Wiener Filter: Specializing to $G = \mathbf{SO}(3)$, $M = \mathbf{S}^2$

The Wiener filter is now specialized to the action of the rotation group $G = \mathbf{SO}(3)$ on the unit sphere $M = \mathbf{S}^2$. The irreducible representations of the rotation group are discussed in Appendix IX.A. The set of irreducible inequivalent representations of $\mathbf{SO}(3)$ is indexed by positive integers. Thus $\pi \in \hat{G}$ is denoted as π_n for $n \in \{0, 1, 2, \ldots\}$, with π_n denoting the $2n+1$ dimensional representation. Also, V_π, W_π and d_π are denoted as V_n, W_n and d_n henceforth.

The fixed point x_0 on the unit sphere is chosen to be the north pole $(0,0,1) \in \mathbb{R}^3$. The stabilizer subgroup H then corresponds to all rotations of the sphere about the Z-axis and the subspace W_n of all vectors fixed by H is one-dimensional space spanned by a single vector; let $e_{n,0}$ denote that vector. This holds for every π_n and thus $d_{\pi_n}^0 = 1$ for all n. The singleton set $\{e_{n,0}\}$ can be extended using Gram-Schmidt procedure to construct an orthonormal basis $\{e_{n,-n}, \ldots, e_{n,0}, \ldots, e_{n,n}\}$ for the $(2n+1)$-dimensional representation space V_n of representation π_n. In this basis, each of $\tilde{\phi}_j, \tilde{\psi}_{ij}$ and $\tilde{l}_i$ is a scalar, as discussed in Section IV. Consequently, the system of equations in (16) reduces to a matrix equation which is much easier to solve than the system of equations in Lemma 1. These quantities are computed using the spherical harmonics as discussed below.

Let $x = [x_1\ x_2\ x_3]'$ be a point on the unit sphere and let $g = \gamma(x)$ be the rotation that rotates the north pole to the point x. Then the irreducible representation, $\tilde{\pi}_n$, corresponding to this rotation is given as (see [26])

$$\begin{aligned} \tilde{\pi}_n(g) &= \tilde{\pi}_n(\gamma(x)) \\ &= \sum_{r=0}^n (-1)^{n-r} \binom{n}{r}^2 \left|\frac{1+x_3}{2}\right|^r \left|\frac{1-x_3}{2}\right|^{(n-r)} \end{aligned} \tag{17}$$

Define functions ρ_n on the unit sphere $\mathbf{S}^2$ as

$$\rho_n(x) = \tilde{\pi}_n(\gamma(x)).$$

The functions ρ_n are the *spherical harmonics* and the *spherical harmonic coefficients* for $\phi_j(g) = R_j(x_0, g\cdot x_0)$ at the frequency $\pi = \pi_n$ is computed as

$$\begin{aligned} \tilde{\phi}_j(\pi_n) &= \int_{\mathbf{SO}(3)} R_j(x_0, g\cdot x_0)\, \tilde{\pi}_n^*(g)\, dg \\ &= \int_{\mathbf{S}^2} R_j(x_0, x)\rho_n(x) d\sigma(x) \end{aligned} \tag{18}$$

where $d\sigma$ denotes integration with respect to the normalized area measure on $\mathbf{S}^2$,

$$d\sigma(x) = \frac{dx_1 dx_2}{|x_3|}, \quad x_1^2 + x_2^2 + x_3^2 = 1. \tag{19}$$

Similarly

$$\tilde{\psi}_{ij}(\pi_n) = \int_{\mathbf{S}^2} R_{ij}(x_0, x)\rho_n(x) d\sigma(x). \tag{20}$$

Recall that R_j and R_{ij} are the correlation functions and the normal equations in Lemma 1 are specialized to

$$\tilde{\phi}_j(\pi_n) = \sum_{i=1}^k \tilde{\psi}_{ij}(\pi_n)\tilde{l}_i(\pi_n)$$

where $\tilde{\pi}_n, \tilde{\phi}_j$ and $\tilde{\psi}_{ij}$ are scalars given by (17), (18), and (20), respectively. The normal equations are solved for $\hat{l}_i(\pi_n)$ and the inverse Fourier transform of $\hat{l}_i(\pi_n)$ gives

$$L_i(x,y) = \sum_{n=0}^\infty (2n+1)\hat{l}_i(\pi_n)\pi_n(\gamma(x)^{-1}\gamma(y)), \tag{21}$$

for $1 \le i \le k$. The coefficient functions $\{L_i(x,y)\}_{i=1}^k$ comprise the spherical Wiener filter and yield the MMSE estimator of ξ based on the η's as outlined in (9).

VI. Matched Filtering on Homogeneous Spaces

A matched filter is developed on a homogeneous space using the Peter-Weyl expansion for square-integrable functions on the associated compact Lie group G. The convolutional integrals defined on the manifold are first expressed as integrals on the group which are then expressed as an infinite sum in Fourier domain. The expressions for signal power and noise variance in the Fourier domain can be simplified using the complexity reduction result of Section IV.

A. Expression for the Signal and the Noise Power in Terms of Integrals Over the Group G

Given the origin x_0 on M, make the following substitutions in (3)

$$\theta(g) = s(g \cdot x_0)$$
$$\phi(g) = h(g \cdot x_0).$$

Using the change of measure formula, the signal component of the filtered output can be expressed as an integral over the group G,

$$\eta_s = \int_M h(x)s(x)dx = \int_G \phi(g)\theta(g)dg. \tag{22}$$

Similarly, the noise power is expressed as an integral on $G \times G$,

$$\begin{aligned}\mathbb{E}[|\eta_v|^2] &= \int_{M\times M} K(x_1,x_2)\, h(x_1)\, h(x_2)\, dx_1\, dx_2 \\ &= \int_{G\times G} K(g_1\cdot x_0, g_2\cdot x_0) h(g_1\cdot x_0) h(g_2\cdot x_0)\, dg_1\, dg_2 \\ &= \int_{G\times G} K\big(g_2^{-1}g_1\cdot x_0, x_0\big)\, h(g_1\cdot x_0) h(g_2\cdot x_0)\, dg_1\, dg_2 \\ &= \int_{G\times G} k\big(g_2^{-1}g_1\big)\ \phi(g_1)\, \phi(g_2)\, dg_1\, dg_2 \end{aligned} \tag{23}$$

where $k(g) = K(g\cdot x_0, x_0)$. Note that the G-invariance property of the noise kernel is used to obtain the expression in (23) for the noise power. These substitutions are important since the Fourier transform on the group G allows the signal and the noise powers to be expressed as discrete sums thereby making the maximization easier.

B. Expressions for the Signal and the Noise Power in the Fourier Domain

Using the Parseval's relation from (7), the signal component is expressed in terms of the Fourier transform coefficients as

$$\eta_s = \sum_{\pi\in\hat{G}} d_\pi\, \mathrm{Tr}(\hat{\phi}_\pi \hat{\theta}_\pi^*) \tag{24}$$

where $\hat{\phi}_\pi = \langle \phi, \pi\rangle$ and $\hat{\theta}_\pi = \langle \theta, \pi\rangle$. The noise power is expressed as

$$\mathbb{E}[|\eta_r|^2] = \sum_{\pi\in\hat{G}} d_\pi\, \mathrm{Tr}(\hat{\phi}_\pi^* \hat{k}_\pi \hat{\phi}_\pi) \tag{25}$$

where $\hat{k}_\pi = \langle k, \pi\rangle$. The following result states that each of the terms in the computation of the trace in (25) is non-negative. This is consistent with the interpretation of each term in the trace as the variance of projection of noise onto the subspaces of the representation space V_π.

Lemma 2: For each $\pi \in \hat{G}$, $\hat{k}_\pi$ is positive semidefinite.

Proof: See Appendix IX.D. ∎

Note that the correlation functions ϕ and θ are H-invariant and the noise correlation kernel k is H-bi-invariant. Thus as outlined in Section IV the size of the summations in the expressions for the signal and the noise power can be reduced. This becomes clearer in the next section when specialized to the sphere.

C. Spherical Matched Filter

The matched filter is now specialized to the action of the rotation group $G = \mathbf{SO}(3)$ on the unit sphere $M = \mathbf{S}^2$. Proceeding as in Section VI.C, fixing the north pole of the unit sphere results in $d^0_{\pi_n} = 1$ for all n. The subspace W_n of all vectors fixed by H is one-dimensional space. The unit vector spanning W_n is extended to construct an orthonormal basis $\{e_{n,-n}, \ldots, e_{n,0}, \ldots, e_{n,n}\}$ for the representation space V_n. In this basis, the signal amplitude (24) can be expressed as

$$\eta_s = \sum_{n=0}^{\infty} \sum_{j=-n}^{n} d_n \hat{\phi}_{n,j} \hat{\theta}^*_{n,j}$$

where $\hat{\phi}_{n,j} = \langle e_{n,0}, \hat{\phi}_n e_{n,j}\rangle$ and $\hat{\theta}_{n,j} = \langle e_{n,0}, \hat{\theta}_n e_{n,j}\rangle$. Owing to H-invariance of ϕ and θ, only the row corresponding to $e_{n,0}$ is involved in the expression, as discussed in Section IV. Similarly the expression for noise power (25) is simplified to

$$\mathbb{E}[|\eta_r|^2] = \sum_{n=0}^{\infty} \sum_{j=-n}^{n} d_n \lambda_n |\hat{\phi}_{n,j}|^2$$

where $\lambda_n = \langle e_{n,0}, k_n e_{n,0}\rangle$. Again, it is due to the H-bi-invariance of k that the noise power has been expressed in a basis in which only one matrix element of the noise spectral density matrix $\hat{k}_n$ is involved.

The matched filter is now given by the function ϕ that maximizes the ratio,

$$\mathrm{SNR}(\phi) = \frac{|\sum_{n,j} d_n \hat{\phi}_{n,j} \hat{\theta}^*_{n,j}|^2}{\sum_{n,j} d_n \lambda_n |\hat{\phi}_{n,j}|^2}.$$

Assuming λ_n's are non zero, the application of Cauchy-Schwarz inequality gives the upper bound on the SNR,

$$\mathrm{SNR}(\phi) \le \sum_{n,j} d_n \lambda_n^{-1} |\hat{\theta}_{n,j}|^2$$

where the equality holds if and only if $\hat{\phi}_{n,j} = \lambda_n^{-1}\hat{\theta}_{n,j}$. However, if some of the λ_n's are zero then consider the set $\Lambda = \{n : \lambda_n = 0\}$. There are two possible cases now: If $\hat{\theta}_{n,j} \neq 0$ for some $n \in \Lambda$ and some $j \in \{0, \pm 1, \pm 2, \ldots, \pm n\}$, then infinite SNR is achieved by choosing $\hat{\phi}_{n,j} = \hat{\theta}_{n,j}\ \forall n \in \Lambda$ and $\hat{\phi}_{n,j} = 0\ \forall n \notin \Lambda$. This is equivalent to choosing the filter as the projection of the signal along the zero noise eigenvalue subspace. And if $\hat{\theta}_{n,j} = 0$ for all $n \in \Lambda$ then the SNR is maximized by choosing $\hat{\phi}_{n,j} = \lambda_n^{-1}\hat{\theta}_{n,j}$ for all $n \notin \Lambda$.

The signal and the noise power can be efficiently computed using the spherical Fourier transform. This also allows us to express the impulse response of the matched filter in terms of the spherical harmonics. Recall that in the spherical harmonic basis $\rho_{n,j}(x) = (\pi_n(\gamma(x)))_{j,0} = \langle \pi_n(\gamma(x))e_{n,0}, e_{n,j}\rangle$. The matched filter is, therefore, implemented by first calculating the spherical harmonic coefficients of the template

$$\hat{\theta}_{n,j} = \langle e_{n,0}, \hat{\theta}_n e_{n,j}\rangle = \int_M s(x)\bar{\rho}_{n,j}(x)dx$$

and then computing

$$\begin{aligned} h(x) &= \phi(\gamma(x)) \\ &= \sum_{n=0}^{\infty}\sum_{j=-n}^{n} d_n \hat{\phi}_{n,j}(\pi_n^*(\gamma(x)))_{j,0} \\ &= \sum_{n=0}^{\infty}\sum_{j=-n}^{n} d_n \frac{\hat{\theta}_{n,j}}{\lambda_n}\rho_{n,j}(x). \end{aligned} \tag{26}$$

Finally, the following result provides an interpretation of $\lambda_n = \langle e_{n,0}, k_n e_{n,0}\rangle$.

Lemma 3: The scalars λ_n can be expressed as

$$\lambda_n = \sum_{j=-n}^{n} \mathbb{E}\left|\int_M r(x)\bar{\rho}_{n,j}(x)dx\right|^2.$$

Proof: See Appendix IX.E. ∎

Since $\{\rho_{n,j}\}$ provide an orthonormal eigenbasis for $\mathbf{SO}(3)$-invariant correlation functions (see Appendix IX.A), λ_n is the sum of the variances of the noise component along each eigenvector of the irreducible subspace of the n^{th} representation of $\mathbf{SO}(3)$.

VII. Applications and Experimental Results

This section discusses application of the spherical matched filter and the spherical Wiener filter to visual homing, denoising 3D surface data and processing cosmic microwave background data. Note that the solutions to (26) and (21) are approximated by computing them only up to a specified value of $n \leq B$, for some positive integer B, which is equivalent to assuming that the *bandwidth* of the spherical signals is B (see [21, Ch. 9]).

A. Denoising 3D Surface Data

The denoising performance of the spherical Wiener filter is studied with the 3D Stanford bunny [27]. The ears of the 3D bunny model were cut off to get a star-shaped object and the bunny was resampled on a regular spherical grid centered at $(-0.01, 0.03, 0.005)$. The point cloud of the bunny is shown in Fig. 1(a) and the corresponding spherical height map is shown in Fig. 1(b) for a sphere of radius 0.001. The projection loses some features around the face of the bunny due to slight deviation from being star-shaped. The resampled bunny model is used as the ground-truth and is made available online at [28].

The sequence of spherical mapping and denoising operations is illustrated in Fig. 2. The mesh plot of the original Stanford bunny is shown in Fig. 2(a) and the resampled 3D surface data is shown in Fig. 2(b). The noisy bunny is shown in Fig. 2(c). The samples are regarded as noisy observations on the unit sphere as shown in Fig. 2(d) and are Wiener filtered to recover the denoised bunny in Fig. 2(e). The bandwidth for restoration was chosen to be 128. The restored bunny is projected back into the Cartesian coordinates as shown in Fig. 2(f). A representative restoration is shown in Fig. 3 with an SNR gain of roughly 15 dB from Wiener filtering using a bandwidth of 128.

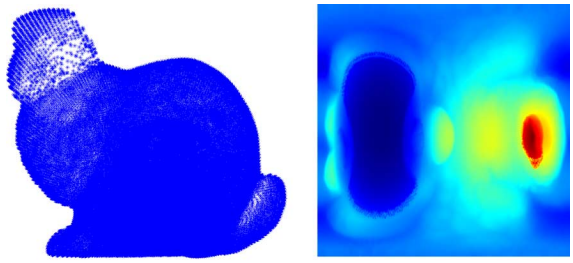

Fig. 1. (a) 3-D bunny image. (b) Height map on a regular spherical grid.

The denoising performance of the Wiener filtering is evaluated with respect to the diffusion-smoothing presented in [10] by comparing the resulting SNR in the filtered images for various initial noisy conditions and bandwidths. It is evident from Fig. 4 that the Wiener filter outperforms diffusion-smoothing at higher bandwidths. However, this improvement with bandwidth is associated with a computational penalty. The fast discrete spherical Fourier transform is computed in $O(B^2 \log^2 B)$ operations [29]. For diffusion-smoothing, the Gauss-Weierstrass kernel with a scale-space factor of 10^{-4} was found to be optimal [10].

B. Visual Homing With a Spherical Matched Filter

This section discusses visual homing of a mobile robot using the omnidirectional images captured by a camera mounted on the robot. The omnidirectional images are publicly available online at [30] and the mobile robot is discussed in [7]. The "original" database consists of 170 omnidirectional images captured at regular grid-points on the floor-plan shown in Fig. 6. The images are all captured in the same orientation with the smallest physical distance between two grid-points being 30 cm.

The objective in visual homing is to trace out a path for a robot from an unknown location in its surroundings to a 'home' location. The navigation is based on the visual information captured by the imaging device mounted on the robot and a prestored *template* image of the scene at the 'home' location. The omnidirectional images used in the experiments are central catadioptric images which can be mapped on to a regular spherical grid since they are equivalent to planar projections of images defined on a sphere [31]. Fig. 5(a) shows an omnidirectional image from the 'original' database captured by the catadioptric sensor mounted on the mobile robot at a grid point. Fig. 5(b) shows the corresponding panoramic scene obtained by unwrapping and cropping the catadioptric image and Fig. 5(c) shows the cropped image mapped on to a sphere.

A simple iterative method for visual homing is proposed based on comparing the given template with the spherical images of the scene observed locally. At each iteration the template is correlated with the images taken at the current grid location and immediate eight-neighbours as shown in Fig. 6. The robot then updates the current location to the location at

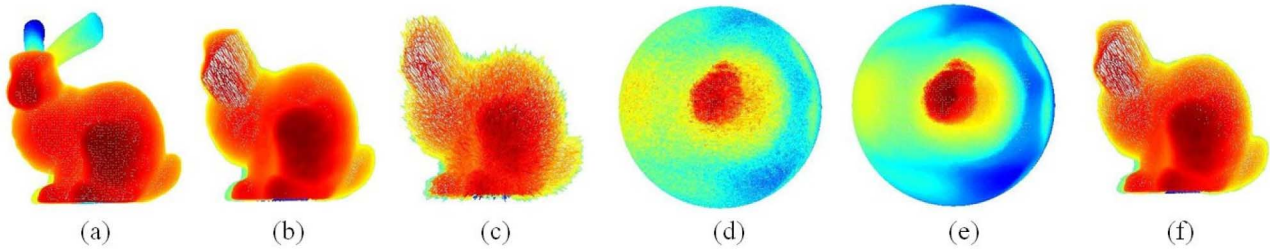

Fig. 2. (a) Original 3D Stanford bunny. (b) 3D bunny (with ears chopped) resampled on a regular spherical grid. (c) Noisy bunny image. (d) Projection of noisy surface data of 3D bunny on the unit sphere. (e) Wiener filtered spherical projection. (f) Restored 3D bunny image.

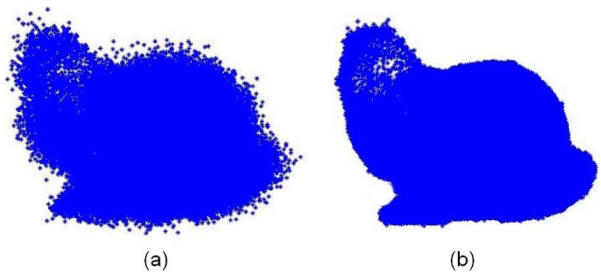

Fig. 3. (a) 3D bunny point cloud with additive noise at an SNR of 15.86 dB. (b) Wiener restored 3D data $(\mathrm{BW} = 128)$ at resulting SNR of 31.39 dB.

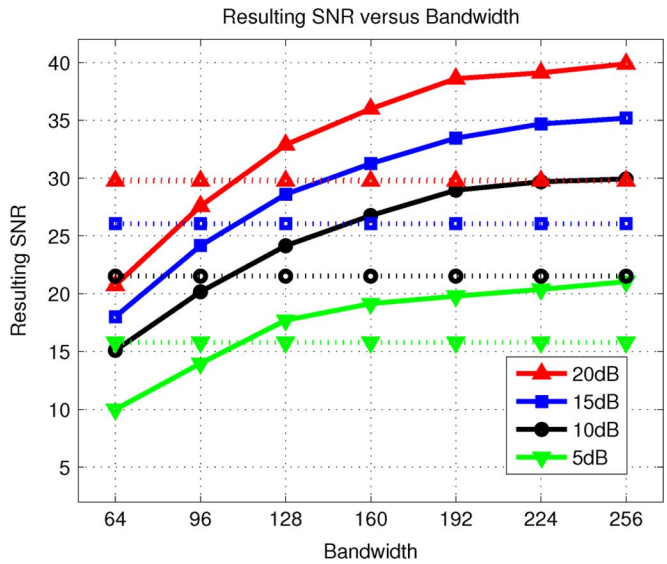

Fig. 4. De-noising performance with respect to the bandwidth for various initial SNR levels. The solid lines represent the resulting SNR with Wiener filtering while the dashed lines shows results with diffusion smoothing [10].

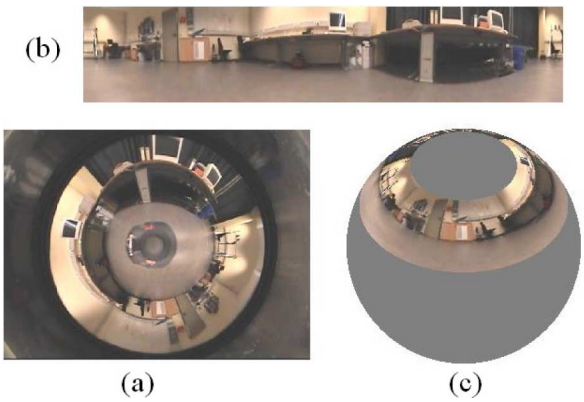

Fig. 5. (a) Catadioptric image captured by a mobile robot; (b) Unwrapped omnidirectional image; (c) Spherical image.

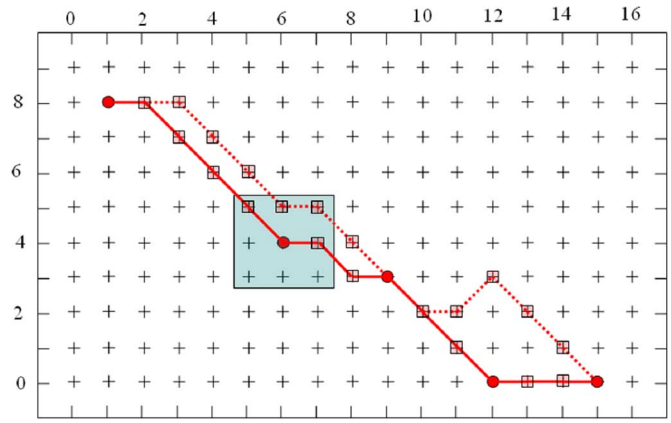

Fig. 6. Grid field of robot's environment [7]. The immediate neighbours of the grid location (4,6) are shown enclosed in the shaded box. The solid red line shows the computed path from (8,1) to (0,15) and the dotted line shows the computed path from (0,15) to (8,1). The panoramic images captured at locations marked with the red dots are shown in Fig. 7.

which the scene matches the closest to the scene in the template. The iterations stop when the current location is not updated. Since the images in the database are captured with the same angular orientation of the robot to the surroundings, it avoids accounting for possible rotations of the spherical images and compensating for the distortion introduced by rotations. We address the more general case in [32] and [33].

Fig. 6 shows the computed path, in solid line, starting at the position (8,1) on the grid and seeking the 'home' location (0,15). The panoramic images of the scene observed by the robot at the points marked with red dots along the path in Fig. 6 are shown in Fig. 7. With the starting position and home location reversed, the computed path is shown in dotted lines in Fig. 6. The video sequences of the scenes captured by the robot (initialized randomly in the grid field) as it traces out its path to the goal are available online at [34] along with the companion source code.

An important metric of performance for visual homing methods is the *return ratio*, which is defined to be the probability that the robot finds the home location when initialized randomly at any point in the grid. The return ratio is associated with every grid point and the average return ratio over the grid allows for a comparison of the performance of our method with other approaches. Table I compares the average return ratios at various subsampling factors for the group theoretical method described in this section and the first-order differential homing

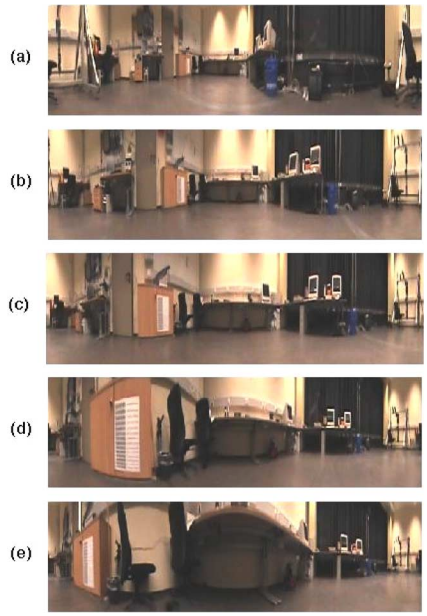

Fig. 7. Omnidirectional scenes captured by mobile robot at grid locations (a) (8,1), (b) (4,6), (c) (3,9), (d) (0,12), and (e) (0,15).

TABLE I
COMPARING DIFFERENTIAL VISUAL HOMING [7] AND OUR GROUP THEORETICAL METHOD IN TERMS OF THE RETURN RATIO AT VARIOUS SUB-SAMPLING RATES AND PSNR OF 10 DB

Sub-sampling factor	1	2	3	4	5
Differential Visual Homing	0.861	0.780	0.671	0.592	0.544
Group theoretical homing	**0.943**	**0.903**	**0.840**	**0.781**	**0.710**

technique put forth in [7]. The simulations were carried out with additive white Gaussian noise at a noise level corresponding to peak-signal-to-noise ratio (PSNR) of 10 dB.

C. Detecting Embedded Objects in Stochastic Background

This section demonstrates the application of matched filtering to the detection of compact objects in a stochastic background of the cosmic microwave radiation collected in all directions of the sky [1]. The cosmic microwave background (CMB) radiation is a form of electromagnetic radiation that fills the entire universe. It was first reported in 1965 by Penzias and Wilson [35]. It has a thermal 2.725 Kelvin black body spectrum which peaks in the microwave range at a frequency of 160.2 GHz corresponding to a wavelength of 1.9 mm. Most cosmologists consider this radiation collected on the celestial sphere to be the best evidence for the Big Bang model of the universe and also refer to it as the relic radiation. In 1970, Sunyaev and Zeldovich [36] reported small-scale fluctuations of the CMB radiation and attributed it to localized foreground emission due to point sources or hot intergalactic gases. This phenomenon is referred to as Sunyaev-Zeldovich (SZ) effect. Analyzing these foreground emissions and separating the embedded sources that cause these emissions is important not only for better understanding of the cosmic structure but also for cleaning up the background CMB radiation.

Several works in the past have employed 2-dimensional planar image processing techniques to filter the CMB data and recover the foreground emission sources [37], [38]. The observations made on small patches of the celestial sphere are assumed to be almost flat and are analyzed using planar matched filters [38] or wavelets [39], [40].

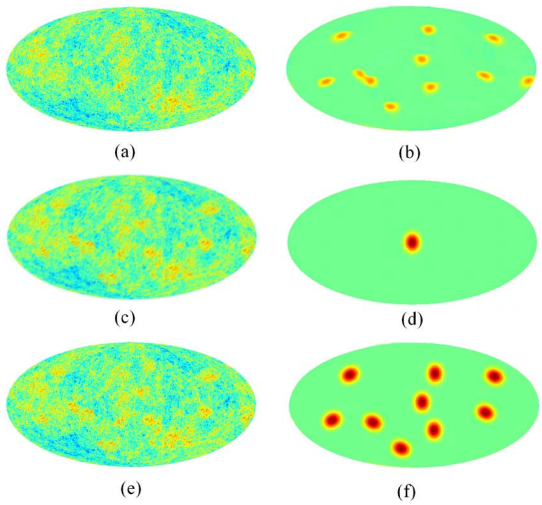

Fig. 8. Detecting compact embedded objects in stochastic background: (a) Map of cosmological microwave background (CMB) simulated in accordance with the CMB power spectrum from WMAP [1]. (b) Compact embedded point sources at different orientations. (c) Simulated sky with embedded objects distorted with motion blur and corrupted with isotropic noise. (d) Gaussian template for the matched filter to detect embedded sources. (e) Wiener filtered image. (f) Objects detected using the Gaussian template.

The templates used for simulating the SZ effect are point sources of fixed sizes. The embedded sources are modelled as $s_i(x) = A_i\tau_i(x)$, where $\tau_i(x)$ is dilated and rotated version of the point-template profile $\tau(x)$. The peak value of A_i determines the SNR $= A_i/(\sigma^2 + B_{\mathrm{CMB}})$ where B_{CMB} is root mean square (rms) value of the background process. The background process in the simulations can be described by the best fit CMB power spectrum as obtained from the data collected by WMAP [1]. Fig. 8(a) shows the simulated map for the background process. The actual foreground objects on the sphere are shown in Fig. 8(b) and are embedded in the background process to yield a simulation of the celestial sky. The simulated skymap undergoes Gaussian motion blur. The resulting observation with additive isotropic white noise of variance $\sigma^2 = 0.01$ is shown in Fig. 8(c). The point template for the matched filter is shown in Fig. 8(d). The noisy spherical image is first Wiener filtered [22], [23] (see Fig. 8(e)) and then the matched filtering is employed to detect the embedded point sources. The locations of the detected objects are shown in Fig. 8(f). Note that the detection was not perfect; the fixed size template was unable to resolve a pair of sources and a weak source along the edge was missed.

Besides the SNR, other factors that affect the detection performance include the size of the point-template and the threshold for the matched filter. The performance of the matched filter also depends on the number of spherical harmonics computed. Given the bandwidth B, the resulting angular resolution is $2\pi/B$ radians for ϕ and π/B radians for θ. The matched filter is designed for increments of θ and ϕ roughly equal to 6 degrees and 12 degrees, respectively, corresponding to $B = 96$. Various software packages are available online for computing the spherical Fourier transform. The Healpix[2] package was used for the tessellation of the sphere [41].

[2]http://healpix.jpl.nasa.gov

VIII. Conclusion

This paper presented the Wiener filter and matched filter for isotropic signal fields on homogeneous spaces. The filters were specialized to the spherical signal spaces under the action of the rotation group. These techniques were applied to the problem of autonomous visual homing in robotics, denoising of 3D surface data in computer graphics and to the detection of point sources embedded in the cosmic microwave background data. These methods incorporate the geometry of the data in the formulation and provide better performance results.

Appendix

A. Irreducible Representations of $\mathbf{SO}(3)$

The rotation group acting on $\mathbb{R}^3$ with respect to the standard Euclidean basis for $\mathbb{R}^3$ corresponds to the special orthogonal group $\mathbf{SO}(3)$, the group of all 3×3 orthogonal matrices with real entries and unit determinant. The representations of $\mathbf{SO}(3)$ are studied as a subset of the representations of the special unitary group $\mathbf{SU}(2)$, comprising all 2×2 complex unitary matrices with unit determinant.

1) Parameterizing Through $\mathbf{SU}(2)$: In this section, we first discuss how a 2×2 special unitary matrix induces the rotation of a point $x = (x_1, x_2, x_3)$ on the sphere by an angle θ about a given axis. The group $\mathbf{SU}(2)$ is the double cover of $\mathbf{SO}(3)$ (there is a two-to-one surjective homomorphism from $\mathbf{SU}(2)$ to $\mathbf{SO}(3)$) and it acts on $\mathbf{S}^2$ as follows. For $x \in \mathbb{R}^3$ define the Hermitian matrix

$$\Phi(x) = \begin{pmatrix} x_3 & x_1 - ix_2 \\ x_1 + ix_2 & -x_3 \end{pmatrix}, x^T = (x_1, x_2, x_3).$$

Φ is a linear isomorphism from $\mathbb{R}^3$ onto the real linear space of 2×2 Hermitian matrices of zero trace and $\det \Phi(x) = -(x_1^2 + x_2^2 + x_3^2)$. For any $U \in \mathbf{SU}(2), U\Phi(x)U^H$ is again a unitary matrix with trace zero and thus of the form $\Phi(x')$ for some $x' \in \mathbb{R}^3$. Also $\det(\Phi(x')) = \det(U)\ \det(\Phi(x))\ \det(U^H) = \det(\Phi(x))$, which implies $x_1^2 + x_2^2 + x_3^2 = {x'_1}^2 + {x'_2}^2 + {x'_3}^2$. Thus, x' is another point on the sphere and x has been rotated to x'. The map $x \mapsto x'$ is therefore a linear isometry. The connectedness of $\mathbf{SU}(2)$ implies that this isometry is a proper rotation R which, in particular, leaves $\mathbf{S}^2$ invariant, thus $R \in \mathbf{SO}(3)$. The unitary matrix U and the corresponding rotation matrix R are connected by $\Phi(R \cdot x) = U\Phi(x)U^H$.

2) Measurable Cross-Section $\gamma : M \to G$: Choose the north pole $x_0 = (0, 0, 1) \in \mathbf{S}^2$ as the sphere's origin and define the map $\gamma : \mathbf{S}^2 \to \mathbf{SO}(3)$ to be the rotation that takes the origin x_0 to x. The expression for the unitary matrix $U_{\gamma(x)}$ associated with the rotation $\gamma(x)$ is obtained by solving $\Phi(x) = U\Phi(x_0)U^H$

$$U_\gamma(x) = \begin{pmatrix} \alpha(x) & \beta(x) \\ -\bar{\beta}(x) & \bar{\alpha}(x) \end{pmatrix} \tag{27}$$

where $\alpha(x) = \left(\frac{1 + x_3}{2}\right)^{1/2}, \beta(x) = -\frac{x_1 - ix_2}{[2(1 + x_3)]^{1/2}}$.

3) Irreducible Representations of $\mathbf{SO}(3)$: The irreducible representations of $\mathbf{SO}(3)$ have been well studied [24] and are discussed here briefly. The irreducible representations of $\mathbf{SO}(3)$ are denoted as π_n for $n \in \mathbb{Z}_{\geq 0}$. The representation space of π_n is the vector space V_n of all homogeneous polynomials of degree $2n$ in two variables (z_1, z_2). A basis for V_n is $\mathcal{B}_n = \{e_{n,j} : n \in \mathbb{Z}_{\geq 0}, j = -n, \ldots, 0, \ldots, n\}$ where

$$e_{n,j}(z_1, z_2) = \frac{z_1^{n+j} z_2^{n-j}}{\sqrt{(n+j)!}\sqrt{(n-j)!}}.$$

The action of $\pi_n(R)$, for $R \in \mathbf{SO}(3)$, on an element $p(\mathbf{z}) \in V_n$ is given as $\pi_n(R)p(\mathbf{z}) = p(U^{-1}\mathbf{z})$, where $U \in \mathbf{SU}(2)$ is the 2×2 unitary matrix that induces the rotation R on $\mathbb{R}^3$, as discussed above.

4) The Basis for $\mathscr{L}^2(\mathbf{S}^2)$: Let $x_0 = (0, 0, 1)$ denote the north pole of the unit sphere. Then the subgroup H of rotations that leave x_0 fixed is the set of rotations about the z axis; let $R_z(\theta)$ denote such a rotation by an angle θ. This rotation corresponds to the unitary matrix $U_z(\theta) = \begin{pmatrix} e^{-j\theta/2} & 0 \\ 0 & e^{j\theta/2} \end{pmatrix}$. The action of the representation π_n corresponding to $R_z(\theta)$ on the basis vector $e_{n,m}$ is given as

$$\pi_n(R_z(\theta))e_{n,m} = e_{n,m}\left(U_z^{-1}(\theta)\,\mathbf{z}\right) = e^{im\theta}e_{n,m}. \tag{28}$$

It follows that the only vectors of V_n that are preserved under $\pi_n(h)$ for all $h \in H$ are the constant multiples of $e_{n,0}$. In other words, W_n is one-dimensional. The matrices $\pi_n(\cdot)$ can be explicitly found by solving (28) above (see [21, ch. 9] for some examples). For $x \in \mathbf{S}^2$, define

$$\rho_{n,j}(x) = (\pi_n(\gamma(x)))_{j,0} = \langle \pi_n(\gamma(x))e_{n,0}, e_{n,j} \rangle$$

where $|j| \leq n$ and $n \in \mathbb{Z}_{\geq 0}$. The functions ρ are the *spherical harmonics* for which we have the following result [26].

Theorem 2: $\{\sqrt{2n+1}\,\rho_{n,j} : j = 0, \pm 1, \ldots, \pm n, n \in \mathbb{Z}_{\geq 0}\}$ is a complete orthonormal basis for $\mathscr{L}^2(\mathbf{S}^2)$. If $K(x_1, x_2)$ is any $\mathbf{SO}(3)$ invariant kernel on $\mathbf{S}^2 \times \mathbf{S}^2$ then $\rho_{n,j}$ are the eigenfunctions of K.

This completes the description of the orthonormal basis for $\mathscr{L}^2(\mathbf{S}^2, d\mathbf{S})$ where the measure $d\mathbf{S}$ is the invariant area measure $d\mathbf{S}(\theta, \phi) = \sin\theta\, d\theta\, d\phi$.

B. Proof of Theorem 1

Proof: Taking the Fourier transform on both sides of $f(g) = f(gh)$ and using the properties of a Haar measure and the fact that representations are homomorphism (which implies that $\pi(gh) = \pi(g)\pi(h), \pi(g^{-1}) = \pi^{-1}(g) = \pi^*(g)$),

$$\begin{aligned}
\hat{f}(\pi) &= \int_G f(gh)\pi^*(g)dg \\
&= \int_G f(g')\pi^*(g'h^{-1})dg' \ (\text{substitute } g' = gh) \\
&= \int_G f(g')(\pi(g')\pi(h^{-1}))^* dg' \\
&= \int_G f(g')\pi^*(h^{-1})\pi^*(g')dg' \\
&= \pi(h)\int_G f(g')\pi^*(g')dg' \\
&= \pi(h)\hat{f}(\pi).
\end{aligned}$$

Integrate both sides with respect to h over H to get $\hat{f}(\pi) = P_\pi \hat{f}(\pi)$ where

$$P_\pi = \int_H \pi(h) dh.$$

Similarly, for an H-bi-invariant function f,

$$\begin{aligned}\hat{f}(\pi) &= \int_G f(h_1 g h_2)\pi^*(g) dg \\ &= \int_G f(g')\pi^*\left(h_1^{-1} g' h_2^{-1}\right) dg' \\ &\quad (\text{substitute } g' = h_1 g h_2) \\ &= \int_G f(g')\pi^*\left(h_2^{-1}\right)\pi^*(g')\pi^*\left(h_1^{-1}\right) dg' \\ &= \pi(h_2)\hat{f}(\pi)\pi(h_1).\end{aligned}$$

Averaging with respect to h_1 and h_2 gives $\hat{f}(\pi) = P_\pi \hat{f}(\pi) P_\pi$. Next, observe that P_π is an orthogonal projection since

$$\begin{aligned}P_\pi^2 &= \left(\int_H \pi(h)\mu_H(dh)\right)^2 \\ &= \int_{H\times H} \pi(h_1 h_2)\mu_H(dh_1)\mu_H(dh_2) \\ &= \int_{H\times H} \pi(h)\mu_H(dh_1)\mu_H(dh) \\ &= \int_H \pi(h)\mu_H(dh) \\ &= P_\pi\end{aligned}$$

and

$$\begin{aligned}P_\pi^* &= \int_H \pi^*(h)\mu_H(dh) \\ &= \int_H \pi(h^{-1})\mu_H(dh) \\ &= \int_H \pi(h')\mu_H(dh') \\ &= P_\pi.\end{aligned}$$

Note that we have used the fact here that the left and right Haar measure on a compact group agree. It remains to show that the $\text{Range}(P_\pi) = W_\pi$. Let $x \in W_\pi$. Then $\pi(h)x = x$ for all $h \in H$. Integrate with respect to h to get $x = P_\pi x \in \text{Range}(P_\pi)$. This implies that $W_\pi \subseteq \text{Range}(P_\pi)$. Next, let $x \in \text{Range}(P_\pi)$. Then $x = P_\pi u$ for some $u \in V_\pi$. For $h \in H$,

$$\pi(h)x = \pi(h)P_\pi u = \int_H \pi(hh')u\, dh' = P_\pi u = x.$$

Thus, $x \in W_\pi$, and $\text{Range}(P_\pi) \subseteq W_\pi$. This completes the proof. ∎

C. Proof of Lemma 1

Proof: Take the Fourier transform on both sides of (13) to get

$$\begin{aligned}\hat{\phi}_j(\pi) &= \int_G \sum_{i=1}^k \left(\int_G l_i(g')\psi_{ij}(g'^{-1}g)\, dg'\right)\pi^*(g)\, dg \\ &= \sum_{i=1}^k \int_{G\times G} l_i(g')\psi_{ij}(g'^{-1}g)\pi^*(g)\, dg' dg \\ &= \sum_{i=1}^k \int_{G\times G} l_i(g')\psi_{ij}(h)\pi^*(g'h)\, dg' dh \\ &= \sum_{i=1}^k \int_{G\times G} l_i(g')\psi_{ij}(h)\pi^*(h)\pi^*(g')\, dh\, dg' \\ &= \sum_{i=1}^k \int_G \psi_{ij}(h)\pi^*(h) dh \int_G l_i(g')\pi^*(g')\, dg' \\ &= \sum_{i=1}^k \hat{\psi}_{ij}(\pi)\hat{l}_i(\pi)\end{aligned}$$

which yields the result. ∎

D. Proof of Lemma 2

Proof: To see that $\hat{k}_\pi$ is positive semidefinite, expand $\langle \hat{k}_\pi x, x\rangle$ to get

$$\begin{aligned}&\left\langle \left(\int_{G\times G} K(g_1\cdot x_0, g_2\cdot x_0)\pi^*\left(g_2^{-1}g_1\right) dg_1 dg_2\right)x, x\right\rangle \\ &= \left\langle \left(\int_{G\times G} \mathbb{E}[r(g_1\cdot x_0)r(g_2\cdot x_0)]\pi^*(g_1)\pi(g_2) dg_1 dg_2\right)x, x\right\rangle \\ &= \int_{G\times G} \langle (\mathbb{E}[r(g_1\cdot x_0)r(g_2\cdot x_0)]\pi(g_2))x, \pi(g_1)x\rangle dg_1 dg_2 \\ &= \int_{G\times G} \mathbb{E}[\langle r(g_2\cdot x_0)\pi(g_2)x, r(g_1\cdot x_0)\pi(g_1)x\rangle] dg_1 dg_2 \\ &= \mathbb{E}\left[\left\langle \int_G r(g_2\cdot x_0)\pi(g_2) dg_2 x, \int_G r(g_1\cdot x_0)\pi(g_1) dg_1 x\right\rangle\right] \\ &= \mathbb{E}\left[\left|\left(\int_G r(g\cdot x_0)\pi(g) dg\right)x\right|^2\right]\end{aligned}$$

which is a nonnegative number. ∎

E. Proof of Lemma 3

Proof: Expand $\lambda_n = \langle e_{n,0}, k_n e_{n,0}\rangle$ to get

$$\begin{aligned}\lambda_n &= \left\langle e_{n,0}, \left(\int_{G\times G} K(g_1\cdot x_0, g_2\cdot x_0)\pi_n^*\left(g_2^{-1}g_1\right) dg_1 dg_2\right)e_{n,0}\right\rangle \\ &= \int_{G\times G} K(g_1\cdot x_0, g_2\cdot x_0)\left\langle e_{n,0}, \left(\pi_n^*\left(g_2^{-1}g_1\right)\right)e_{n,0}\right\rangle dg_1 dg_2 \\ &= \int_{G\times G} K(g_1\cdot x_0, g_2\cdot x_0)\left(\bar{\pi}_n\left(g_2^{-1}g_1\right)\right)_{0,0} dg_1 dg_2 \\ &= \int_{G\times G} \mathbb{E}[r(g_1\cdot x_0)r(g_2\cdot x_0)]\sum_{j=-n}^n (\bar{\pi}_n(g_1))_{j,0}(\pi_n(g_2))_{j,0} dg_1 dg_2 \\ &= \sum_{j=-n}^n \int_{M\times M} \mathbb{E}[r(x_1)r(x_2)]\bar{\rho}_{n,j}(x_1)\rho_{n,j}(x_2) dx_1 dx_2 \\ &= \sum_{j=-n}^n \mathbb{E}\left|\int_M r(x)\bar{\rho}_{n,j}(x) dx\right|^2.\end{aligned}$$

Each term in the summation above is the variance of the noise projected onto the subspace spanned by $\rho_{n,j}$. ∎

ACKNOWLEDGMENT

The authors would like to thank K. R. Parthasarathy for several useful discussions and suggestions.

REFERENCES

[1] The WMAP Science Working Group (WSWG), "Wilkinson microwave anistropy probe (WMAP): Three-year explanatory supplement," 2006 [Online]. Available: http://lambda.gsfc.nasa.gov

[2] Y. Yagi, "Omni-directional sensing and its applications," *IEICE Trans. Inf. Syst.*, vol. E82-D, no. 3, Mar. 1999.

[3] T. Svoboda and T. Pajdla, "Panoramic cameras for 3D computation," in *Czech Pattern Recognition Workshop*, Feb. 2000, pp. 63–70.

[4] S. Li, "Full-view spherical image camera," in *Proc. IEEE Int. Conf. Pattern Recogn.*, Aug. 2006, pp. 386–390.

[5] N. D. Jankovic and M. D. Naish, "Developing a modular active spherical vision system," in *Proc. IEEE Int. Conf. Robot. Autom.*, Apr. 2005, pp. 1234–1239.

[6] C. Pegard and E. M. Mouaddib, "A mobile robot using a panoramic view," in *Proc. IEEE Int. Conf. Robot. Autom.*, Apr. 1996, pp. 89–94.

[7] A. Vardy and R. Möller, "Biologically plausible visual homing methods based on optical flow techniques," *Connection Sci.*, vol. 17, pp. 47–89, Mar. 2005.

[8] R. Orghidan, E. M. Mouaddib, and J. Salvi, "Omnidirectional depth computation from a single image," in *Proc. IEEE Int. Conf. Robot. Autom.*, Apr. 2005, pp. 1222–1227.

[9] R. Orghidan, J. Salvi, and E. M. Mouaddib, "Accuracy estimation of a new omnidirectional 3D vision sensor," in *Proc. IEEE Int. Conf. Image Process.*, Sep. 2005, pp. 365–368.

[10] T. Bulow, "Spherical diffusion for 3D surface smoothing," *IEEE Trans. Pattern Anal. Mach. Intell.*, Dec. 2004.

[11] K. Zhou, H. Bao, and J. Shi, "3D surface filtering using spherical harmonics," in *Computer-Aided Design*. New York: Elsevier, 2004, vol. 36, pp. 363–375.

[12] H. Li and R. Hartley, "Conformal spherical representation of 3D genus-zero meshes," *Pattern Recogn.*, vol. 40, no. 10, pp. 2742–2753, 2007.

[13] A. M. Bronstein, M. M. Bronstein, and R. Kimmel, "Expression-invariant representations of faces," *IEEE Trans. Image Process.*, vol. 16, no. 1, pp. 188–197, Jan. 2007.

[14] J. H. Manton, "Optimization algorithms exploiting unitary constraints," *IEEE Trans. Signal Process.*, vol. 50, pp. 635–650, Mar. 2002.

[15] R. Mahony and J. H. Manton, "The geometry of the Newton method on non-compact Lie groups," *J. Global Optimiz.*, vol. 23, no. 3, pp. 309–327, 2002.

[16] R. Arora, "On learning rotations," *Adv. Neural Inf. Process. Syst.*, 2009.

[17] W. Moran and J. H. Manton, *Group Theory in Radar and Signal Processing*. New York: Kluwer, 2003.

[18] J. H. Manton, "On the role of differential geometry in signal processing," in *Proc. IEEE Int. Conf. Acoust., Speech, Signal Process.*, Mar. 2005, vol. 5, pp. v/1021–v/1024.

[19] B. Yazici, "Stochastic deconvolution over groups," *IEEE Trans. Inf. Theory*, vol. 50, no. 3, pp. 494–510, Mar. 2004.

[20] M. Franz and H. Krapp, "Wide-field, motion-sensitive neurons and matched filters for optic flow fields," *Biolog. Cybern.*, vol. 83, pp. 185–197, 2000.

[21] G. S. Chirikjian and A. B. Kyatkin, *Engineering Applications of Noncommutative Harmonic Analysis*. Boca Raton, FL: CRC, 2000.

[22] R. Arora and H. Parthasarathy, "Wiener filter for isotropic signal fields," in *Proc. 41st Asilomar Conf. Signals, Syst., Comput.*, Nov. 2007, pp. 540–544.

[23] R. Arora and H. Parthasarathy, "Spherical Wiener filter," in *Proc. IEEE Int. Conf. Image Process.*, Oct. 2008.

[24] R. Lenz, *Group Thoretical Methods in Image Processing*. Berlin: Springer-Verlag, 1990, LNCS.

[25] W. Burnside, *Theory of Groups of Finite Order*. Cambridge, U.K.: Cambridge Univ. Press, 1997.

[26] E. P. Wigner, *Group Theory and its Applications to the Quantum Mechanics of Atomic Spectra*. New York: Academic, 1959.

[27] Computer Graphics Lab. Stanford Univ. [Online]. Available: http://graphics.stanford.edu/data/

[28] R. Arora, Supplementary Material 2009 [Online]. Available: http://www.cae.wisc.edu/ sethares/links/raman/TSP09/index.html

[29] J. Driscoll and D. Healy, "Computing Fourier transforms and convolutions on the 2-sphere," *Adv. Appl. Math.*, vol. 15, p. 202250, 1994.

[30] A. Vardy and R. Möller, Panoramic Image Database [Online]. Available: http://www.ti.uni-bielefeld.de/html/research/avardy/index.html

[31] C. Geyer and K. Daniilidis, "Catadioptric projective geometry," *Int. J. Computer Vision*, vol. 43, pp. 223–243, 2001.

[32] R. Arora, "Group theoretical methods in signal processing: Learning similarities, transformations and invariants," Ph.D. thesis, Univ. Wisconsin-Madison, , 2009.

[33] R. Arora and H. Parthasarathy, "Navigation using a spherical camera," in *Proc. Int. Conf. Pattern Recogn.*, Dec. 2008.

[34] R. Arora, Visual Homing Videos 2009 [Online]. Available: http://www.cae.wisc.edu/sethares/links/raman/sphnav.html

[35] A. A. Penzias and R. W. Wilson, "A measurement of excess antenna temperature at 4080 mc/s," *Astrophys. J.*, vol. 142, pp. 419–421, 1965.

[36] R. A. Sunyaev and Y. B. Zeldovich, "Small-scale fluctuations of relic radiation," *Astrophys. Space Sci.*, vol. 7, 1970.

[37] M. G. Haehnelt and M. Tegmark, "Using the kinematic Sunyaev-Zel'dovich effect to determine the peculiar velocities of clusters of galaxies," *Mon. Not. Roy. Astron. Soc.*, vol. 279, pp. 545–556, 1996.

[38] M. Tegmark and A. de Oliveira-Costa, "Removing point sources from CMB maps," *Astrophys. J. Lett.*, vol. 500, pp. L83–L86, 1998.

[39] J. L. Sanz, D. Herranz, and E. Martinez-Gonzalez, "Optimal detection of sources on a homogeneous and isotropic background," *Astrophys. J.*, vol. 552, pp. 484–492, 2001.

[40] L. Cayon, J. L. Sanz, R. B. Barreiro, E. Martinez-Gonzalez, P. Vielva, L. Toffolatti, J. Silk, J. M. Diego, and F. Argueso, "Isotropic wavelets: A powerful tool to extract point sources from cosmic microwave background maps," *Mon. Not. Roy. Astron. Soc.*, vol. 315, pp. 757–761, 2000.

[41] K. M. Gorski, E. Hivon, A. J. Banday, B. D. Wandelt, F. K. Hansen, M. Reinecke, and M. Bartelmann, "Healpix: A framework for high-resolution discretization and fast analysis of data distributed on the sphere," *Astrophys. J.*, vol. 622, pp. 759–771, 2005.

Raman Arora (M'07) received the B.Eng. degree in electronics and communication engineering from Netaji Subhas Institute of Technology, New Delhi, India, in 2001, and the M.S. and Ph.D. degrees in electrical engineering from University of Wisconsin-Madison in 2005 and 2009, respectively.

He is currently a Postdoctoral Research Associate with the Electrical Engineering Department, University of Washington, Seattle. From 2001 to 2003, he was with the DSP Group of Hughes Software Systems. His research interests include group theoretical methods in signal processing with applications to acoustics, bio-informatics, and vision.

Harish Parthasarathy received B.Tech. degree in 1990 from the Indian Institute of Technology (IIT) Kanpur, and the Ph.D. degree from IIT, Delhi, in 1994, both in electrical engineering.

He was an Assistant Professor during 1994–1997 with the Electrical Engineering Department, IIT Bombay and during 1997–1998 with the Electrical Engineering Department, IIT Kanpur. He was an Application Engineer with ST MicroElectronics, Delhi, during 1998–2000 before joining Netaji Subhas Institute of Technology, New Delhi, in 2000, where he worked as Assistant Professor until June 2007. Since July 2007, he has been a Professor with the Division of Electronics and Communication Engineering, Netaji Subhas Institute of Technology. His teaching and research interests are in the areas of circuits and systems, signal processing, stochastic nonlinear filters, electromagnetics, and group representations.